Ionization of atomic hydrogen by an intense x-ray laser pulse: An *ab initio* study of the breakdown of the dipole approximation

Thore Espedal Moe and Morten Førre*
Department of Physics and Technology, University of Bergen, 5007 Bergen, Norway

(Received 17 November 2017; published 22 January 2018)

Solving the time-dependent Schrödinger equation numerically within the framework of an *ab initio* model, the breakdown of the dipole approximation in modeling the ionization and excitation dynamics of a hydrogen atom exposed to an intense 1.36-keV x-ray laser pulse is investigated in some detail. The relative importance of the $\boldsymbol{A}^2$ diamagnetic term in comparison with the $\boldsymbol{A}\cdot\boldsymbol{p}$ contribution to the resulting beyond-dipole (nondipole) light-matter interaction is studied for laser pulse intensities ranging from the weak perturbative to the strong-field regime. It is found that the diamagnetic interaction represents by far the most important correction to the dipole approximation at higher field strengths, while nondipole corrections induced by the $\boldsymbol{A}\cdot\boldsymbol{p}$ operator are generally small and largely independent of the laser intensity. The most profound finding of the present study was the discovery of a forward-backward asymmetry in the underlying electron ejection dynamics: Depending on the electron's kinetic energy in the final state, the photoelectron tends to be emitted in the laser propagation (forward) and/or counterpropagation (backward) directions, for energies corresponding to the low-energy and/or high-energy side of the multiphoton resonances, respectively.

DOI: 10.1103/PhysRevA.97.013415

I. INTRODUCTION

The laser is today a workhorse in natural sciences, enabling manipulation and control of physical processes at the atomic level. In the theoretical description of light-matter interactions it is common to impose the so-called dipole approximation, one of the most frequently used approximations in atomic, molecular, and optical physics. In this approximation, the laser field is treated as a homogeneous time-varying electric field and the magnetic-field component and the spatial dependence of the fields are considered unimportant and are therefore disregarded. The dipole approximation is usually valid for longer-wavelength fields, provided the laser intensity is not so high that the magnetic component [1–18] and/or relativistic effects [19–24] inevitably become important. Breakdown of the dipole approximation in strong-field ionization has been experimentally observed in the near- and midinfrared regime [25,26].

In the present work we study the breakdown of the dipole approximation in the multiphoton ionization and excitation dynamics of a hydrogen atom, induced by an intense short-wavelength x-ray laser pulse. The atom is assumed to be irradiated by 1.36-keV photons corresponding to a laser wavelength of 0.91 nm. At such short wavelengths the validity of the dipole approximation is questionable *per se* and the spatial dependence of the vector potential $\boldsymbol{A}(\boldsymbol{r},t)$ modeling the laser pulse must be considered [27]. To understand the importance of different types of effects beyond the dipole approximation, it is common to expand the laser potential $\boldsymbol{A}$ in terms of a Taylor series [12,23,28,29], from which the lowest-order contribution represents the electric dipole interaction where the electric field is assumed to be homogeneous, and any spatial dependences of the fields and magnetic-field effects are ascribed to the higher-order terms in the expansion.

In this work, we go beyond the standard Taylor expansion trick and instead consider the full spatial dependence of the fields. It is found that the diamagnetic interaction $\boldsymbol{A}^2$ represents the most significant source of beyond-dipole-induced dynamics, especially in the strong-field regime, while the $\boldsymbol{A}\cdot\boldsymbol{p}$ interaction takes over as the dominating source of nondipole effects only in the weak-field limit. It is further found that including the leading-order contribution beyond the electric dipole approximation, in both interactions, is sufficient to describe the ionization and excitation dynamics initiated by the laser pulse for all intensities considered here. An interesting finding of the present study is that it is found that the significance of the $\boldsymbol{A}\cdot\boldsymbol{p}$ operator, in terms of nondipole effects, is largely independent of the laser intensity. Nonetheless, by varying the laser intensity clear signatures of beyond-dipole behavior of the system were detected, which could all be attributed to the $\boldsymbol{A}^2$ operator, the most profound one being that the diamagnetic interaction has a strong influence on the direction in which the photoelectron is emitted depending on the kinetic energy of the electron. This rather odd behavior of the system is further explained in terms of a simple model designed to capture the essential features of the underlying ejection dynamics.

Atomic units (a.u.) are used throughout unless stated otherwise.

II. THEORY AND METHODOLOGY

In the nonrelativistic approximation, the time evolution of a particle of mass m and charge q, as represented by the wave function Ψ, moving in a (Coulomb) potential V and laser field

*morten.forre@uib.no

$\boldsymbol{A}$, is governed by the time-dependent Schrödinger equation (TDSE)

$$i\hbar\frac{\partial}{\partial t}\Psi = H\Psi, \tag{1}$$

with the Hamiltonian

$$H = \frac{1}{2m}[\boldsymbol{p} - q\boldsymbol{A}(\eta)]^2 + V(\boldsymbol{r}). \tag{2}$$

The vector potential $\boldsymbol{A}(\eta) = \boldsymbol{A}(\omega t - \boldsymbol{\kappa}\cdot\boldsymbol{r})$ satisfies the wave equation and depends on both space and time coordinates. Here ω is the central angular frequency of the field, $\boldsymbol{\kappa} = \omega/c\ \hat{\boldsymbol{\kappa}}$ is the wave vector, and c is the speed of light. Imposing the Coulomb gauge restriction $\boldsymbol{\nabla}\cdot\boldsymbol{A} = 0$ on the field, the Hamiltonian is cast into the form

$$H = \frac{p^2}{2m} + V - \frac{q}{m}\boldsymbol{A}\cdot\boldsymbol{p} + \frac{q^2}{2m}\boldsymbol{A}^2. \tag{3}$$

While the $\boldsymbol{A}^2$ interaction in Eq. (3) does not contribute to the light-matter dynamics within the dipole approximation, it is known to play an essential role when going beyond the dipole approximation, i.e., when describing beyond-dipole (nondipole) ionization processes in superintense laser fields [1–13]. For example, the main nondipole contribution due to the magnetic field is accounted for by this operator.

In the present work, the laser pulse is modeled in terms of the vector potential

$$\boldsymbol{A}(\eta) = \frac{E_0}{\omega}f(\eta)\sin(\eta+\phi)\hat{\boldsymbol{u}}_p, \tag{4}$$

where E_0 is the electric-field strength at peak intensity, ϕ is the carrier-envelope phase (CEP), $f(\eta)$ defines the laser pulse profile, and $\hat{\boldsymbol{u}}_p$ is a unit vector pointing in the laser polarization direction. Inserting the vector potential (4) into Eq. (3), the Hamiltonian takes the form

$$H = \frac{p^2}{2m} + V - \frac{q}{m}\frac{E_0}{\omega}f(\eta)\sin(\eta+\phi)\hat{\boldsymbol{u}}_p\cdot\boldsymbol{p} + \frac{q^2}{2m}\frac{E_0^2}{\omega^2}f^2(\eta)\sin^2(\eta+\phi). \tag{5}$$

In order to study the relative importance of the two light-matter interaction terms, we also consider the Hamiltonian

$$H = \frac{p^2}{2m} + V - \frac{q}{m}\frac{E_0}{\omega}f(\eta)\sin(\eta+\phi)\hat{\boldsymbol{u}}_p\cdot\boldsymbol{p}, \tag{6}$$

where the last diamagnetic ($\boldsymbol{A}^2$) term has been omitted. In the dipole approximation, the spatial dependence of the vector potential is neglected and Eq. (5) reduces to the much simpler form

$$H_{\rm dip} = \frac{p^2}{2m} + V - \frac{q}{m}\frac{E_0}{\omega}f(t)\sin(\omega t+\phi)\hat{\boldsymbol{u}}_p\cdot\boldsymbol{p} + \frac{q^2}{2m}\frac{E_0^2}{\omega^2}f^2(t)\sin^2(\omega t+\phi). \tag{7}$$

Note that in this dipole limit the last interaction term, i.e., the diamagnetic one, becomes a purely time-dependent factor which effectively cancels out in the TDSE when the gauge transformation

$$\Psi' = \exp\left[\frac{i}{\hbar}\int_{-\infty}^{t}\frac{q^2}{2m}\frac{E_0^2}{\omega^2}f^2(t')\sin^2(\omega t'+\phi)dt'\right]\Psi \tag{8}$$

is imposed. Solving the TDSE with the exact (nonrelativistic) Hamiltonian (5) will typically result in an intractable computational problem due to the coupling of space and time coordinates and therefore instead the dipole approximation (7) is widely used. However, in certain pulse regimes, i.e., in the cases of very short laser wavelengths and/or high-intensity fields, the dipole approximation may no longer be valid and beyond-dipole (nondipole) effects must be accounted for. Now, in order to simplify the theoretical treatment, it is common to assume that the space-dependent vector potential can be expanded in powers of $\boldsymbol{\kappa}\cdot\boldsymbol{r}$, where the term linear in $\boldsymbol{\kappa}\cdot\boldsymbol{r}$ represents the leading-order correction beyond the dipole approximation [1–14]. Keeping only terms up to first order in $\boldsymbol{\kappa}\cdot\boldsymbol{r}$, the nondipole Hamiltonian (5) is cast into the approximate form

$$H \simeq \frac{p^2}{2m} + V - \frac{q}{m}\frac{E_0}{\omega}f(t)\sin(\omega t+\phi)\hat{\boldsymbol{u}}_p\cdot\boldsymbol{p} + \frac{q}{m}\frac{E_0}{\omega}\boldsymbol{\kappa}\cdot\boldsymbol{r}\left[f(t)\cos(\omega t+\phi) + \frac{1}{\omega}\dot{f}(t)\sin(\omega t+\phi)\right]\hat{\boldsymbol{u}}_p\cdot\boldsymbol{p} - \frac{q^2}{2m}\frac{E_0^2}{\omega^2}\boldsymbol{\kappa}\cdot\boldsymbol{r}\left[\frac{2}{\omega}f(t)\dot{f}(t)\sin^2(\omega t+\phi) + f^2(t)\sin(2\omega t+2\phi)\right]. \tag{9}$$

Here we will adopt a sine-squared carrier envelope for the laser field, i.e.,

$$f(\eta) = \begin{cases}\sin^2\left(\frac{\pi\eta}{\omega T}\right) & \text{for } 0<\eta<\omega T\\ 0 & \text{otherwise.}\end{cases} \tag{10}$$

Then $f(t) = \sin^2(\frac{\pi t}{T})$ and $\dot{f}(t) = \frac{\pi}{T}\sin(\frac{2\pi t}{T})$. In the present work, the (total) pulse duration T is chosen sufficiently long so that $f(\eta)\simeq 0$ at times $t=0$ and $t=T$, i.e., the pulse is assumed to be on over the time interval $t\in[0,T]$.

The TDSE is discretized by expanding the three-dimensional wave function on a product basis of hydrogenic radial wave functions R_{kl} and spherical harmonics Y_{lm} as

$$\Psi(\boldsymbol{r},t) = \sum_{klm} c_{klm}(t)R_{kl}(|\boldsymbol{r}|)Y_{lm}(\hat{\boldsymbol{r}}), \tag{11}$$

where both continuum (scattering) and bound states are included in the expansion. The radial wave functions are obtained by diagonalizing the field-free hydrogenic Hamiltonian in a B-spline basis. The matrix representation of the respective light-matter interaction Hamiltonians (5), (7), and (9) is then computed and the resulting system of ordinary differential equations is solved by a predictor-corrector method developed by Gordon and Shampine [30]. For the discretization of the Hamiltonians (7) and (9) we have followed the same approach

as described in Ref. [12]. The corresponding scheme for the Hamiltonian (5) is computationally much more involved because of the coupling of spatial and temporal degrees of freedom and therefore needs special attention.

In setting out to solve the TDSE with the full Hamiltonian (5), the corresponding matrix elements are obtained from

$$\langle \Psi_{k'l'm'}|H|\Psi_{klm}\rangle = \langle R_{k'l'}Y_{l'm'}|\frac{p^2}{2m}+V - \frac{q}{m}\boldsymbol{A}\cdot\boldsymbol{p}+\frac{q^2}{2m}\boldsymbol{A}^2|R_{kl}Y_{lm}\rangle. \quad (12)$$

Here it is the evaluation of the last two terms that causes difficulty when retaining the full space dependence of the vector potential, i.e.,

$$\langle R_{k'l'}Y_{l'm'}|\boldsymbol{A}\cdot\boldsymbol{p}|R_{kl}Y_{lm}\rangle \quad (13)$$

and

$$\langle R_{k'l'}Y_{l'm'}|\boldsymbol{A}^2|R_{kl}Y_{lm}\rangle. \quad (14)$$

In order to perform these calculations the vector potential (4) with the envelope (10) must be translated into a more tractable form. By employing elementary trigonometric identities, the vector potential may be decomposed into a finite sum of products depending separately on space and time,

$$\boldsymbol{A} = \hat{\boldsymbol{u}}_p\frac{E_0}{\omega}\sum_\alpha[C_\alpha(t)\sin(D_\alpha\boldsymbol{k}\cdot\boldsymbol{r})+F_\alpha(t)\cos(G_\alpha\boldsymbol{k}\cdot\boldsymbol{r})], \quad (15)$$

where the time dependences are contained in the functions $C_\alpha(t)$ and $F_\alpha(t)$ and the index α enumerates the terms in the decomposition. Similarly, for $\boldsymbol{A}^2$,

$$\boldsymbol{A}^2 = \frac{E_0^2}{\omega^2}\sum_\beta[C_\beta(t)\sin(D_\beta\boldsymbol{k}\cdot\boldsymbol{r})+F_\beta(t)\cos(G_\beta\boldsymbol{k}\cdot\boldsymbol{r})]. \quad (16)$$

Each space-dependent term in these sums may further be separated into angular and radial parts through the spherical wave expansion of plane waves

$$e^{i\boldsymbol{k}\cdot\boldsymbol{r}} = \cos(\boldsymbol{k}\cdot\boldsymbol{r})+i\sin(\boldsymbol{k}\cdot\boldsymbol{r}) = 4\pi\sum_{L=0}^{\infty}\sum_{M=-L}^{L} i^L j_L(kr)Y^*_{LM}(\Omega_k)Y_{LM}(\Omega_r), \quad (17)$$

where Ω_r and Ω_k denote the angular coordinates of $\boldsymbol{r}$ and $\boldsymbol{k}$, respectively. This expansion allows the angular parts of (13) and (14) to be computed analytically through the relation

$$\langle Y_{l_3m_3}(\Omega_r)|Y_{l_1m_1}(\Omega_r)|Y_{l_2m_2}(\Omega_r)\rangle = \sqrt{\frac{(2l_1+1)(2l_2+1)}{4\pi(2l_3+1)}} \times C(l_1,l_2,l_3|0,0,0)C(l_1,l_2,l_3|m_1,m_2,m_3), \quad (18)$$

where $C(l_1,l_2,l_3|m_1,m_2,m_3)$ are the Clebsch-Gordan coefficients. Due to the conditions for the nonvanishing of the Clebsch-Gordan coefficients, the maximum value of l ($l_{\max}$) used in the construction of the basis wave functions limits the maximum contributing value of L in the expansion (17). The sum in (17) is thus analytically truncated after $L = 2l_{\max}+1$, where the plus one stems from the effect of the $\boldsymbol{p}$ operator on the basis wave function in (13). Having obtained expressions for the angular parts, the radial integrals are then performed by a Gauss-Legendre quadrature and the matrix elements (12) are computed.

III. RESULTS AND DISCUSSION

We have considered a hydrogen $1s$ electron exposed to a 15-cycle (i.e., $T = 15\times 2\pi/\omega$) x-ray laser pulse of angular frequency $\omega = 50$ a.u., which corresponds to 1.36-keV photons. The value of the CEP in Eq. (4) is set to $\varphi = 0$, but we emphasize that the results obtained are vastly independent of the particular choice of phase. The system is solved numerically in a radial box extending to $R_{\max} = 40$ a.u. The hydrogenic radial eigenstates are expanded in terms of 530 sixth-order B-spline functions distributed equidistantly on the interval $r \in [0\ R_{\max}]$ and they are obtained by diagonalization of the corresponding field-free hydrogenic Hamiltonian. In solving the TDSE, 261 of the computed eigenstates are kept in the expansion of the system wave function (11) for each (l,m) channel. This yields a maximum attainable electronic continuum energy of about 210 a.u. in the restricted basis set. Furthermore, the number of angular momenta included in the basis was limited up to $l = l_{\max} = 16$ in the simulations, making the total number of angular channels 289 when all possible values of the magnetic quantum number m are included. The value of the basis parameters was systematically varied in order to control the accuracy and reliability of the computed data.

In the present work, all calculations were executed using both the exact Hamiltonian (5) and its linear approximation (9). As a matter of fact, all results appeared to be largely independent of this choice, i.e., employing the Hamiltonian (5) and/or (9) yielded the same result, simply demonstrating that the linear approximation (9) is valid for the laser parameters considered here.

Figure 1 shows the total ionization probability [Fig. 1(a)], the survival probability in the initial state [Fig. 1(b)], and the total probability of excitation to excited bound states [Fig. 1(c)], as a function of the electric-field strength E_0. Data obtained with the Hamiltonians (5) [or alternatively (9)], (6), and (7) are shown for comparison. The highest field strength considered, $E_0 = 500$ a.u., corresponds to the peak laser intensity $I = 8.8\times 10^{21}$ W/cm^2 and an electron ponderomotive energy U_p of 25 a.u. At this high intensity the ionizing electron's (classical) velocity in the laser field is likely to surpass 7% of the speed of light during the laser interaction. Nevertheless, a nonrelativistic treatment is justified. When it comes to the total ionization probability, as well as the probability of remaining in the initial state, Fig. 1 reveals that nondipole effects start to become visible for field strengths beyond $E_0 \sim 100$ a.u. In contrast, the relative population in excited states turns out to be much more influenced, as the dipole and nondipole results deviate from each other already at $E_0 \sim 1$ a.u. As such, the population in excited states seems to be a sensitive probe for measuring beyond-dipole dynamics. Concerning the relative importance of the two light-atom interaction terms in Eq. (5), and comparing the results obtained by the Hamiltonians (5) and (6), respectively, it is evident from Fig. 1 that it is the

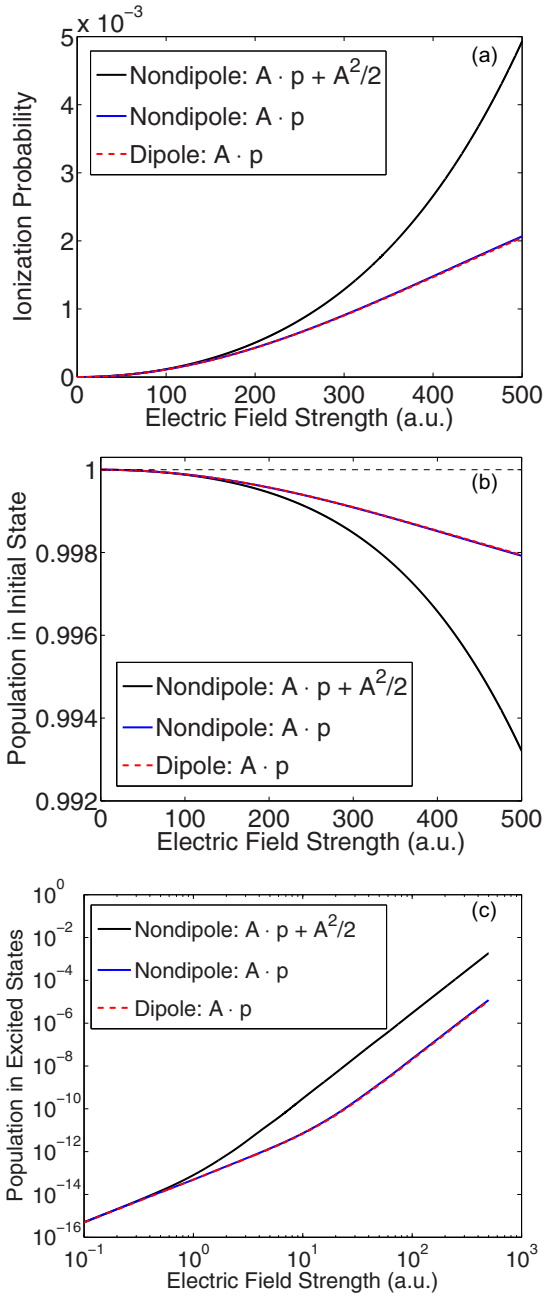

FIG. 1. (a) Total ionization probability vs electric-field strength for a 15-cycle laser pulse with $\omega = 50$ a.u. The solid black line shows the (full) nondipole result obtained by solving the TDSE with the Hamiltonian in Eq. (5), the solid blue line the nondipole result obtained by solving the TDSE with only the $\boldsymbol{A} \cdot \boldsymbol{p}$ term, i.e., the Hamiltonian in Eq. (6), and the dashed red line the dipole approximation result obtained by solving the TDSE with the Hamiltonian in Eq. (7). (b) Corresponding survival probability. (c) Corresponding probability of excitation.

diamagnetic term in Eq. (5), i.e., the $\boldsymbol{A}^2$ interaction, that by far contributes the most to the nondipole dynamics. As a matter of fact, only tiny differences between the dipole results and the results obtained with the Hamiltonian (6) are displayed in the figure. This is in agreement with earlier findings for light in the longer-wavelength (xuv) regime [2,3,12].

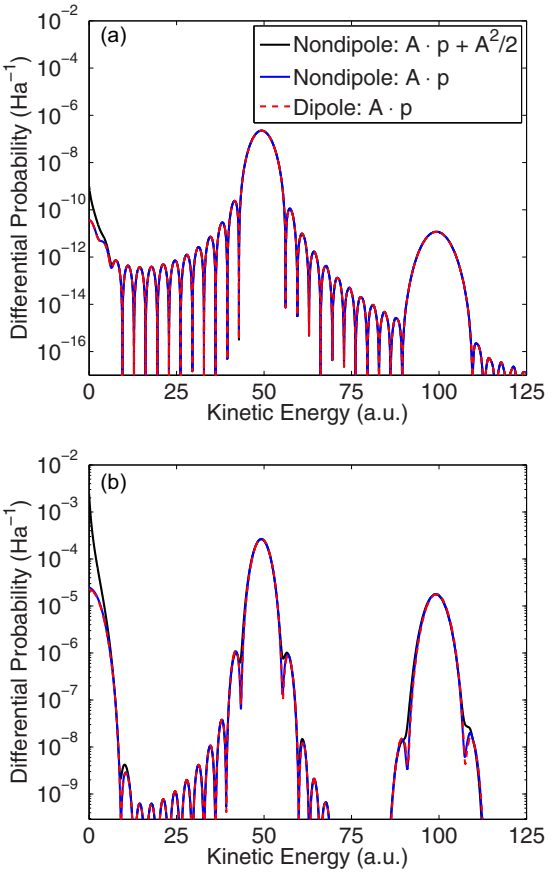

FIG. 2. Kinetic energy spectrum of the emitted photoelectron for a 15-cycle laser pulse with $\omega = 50$ a.u. and for two different electric-field strengths (a) $E_0 = 10$ a.u. and (b) $E_0 = 400$ a.u. The solid black line shows the (full) nondipole result obtained by solving the TDSE with the Hamiltonian in Eq. (5), the solid blue line the nondipole result obtained by solving the TDSE with only the $\boldsymbol{A} \cdot \boldsymbol{p}$ term, i.e., the Hamiltonian in Eq. (6), and the dashed red line the dipole result obtained by solving the TDSE with the Hamiltonian in Eq. (7).

Figure 2 shows the kinetic energy distribution of the emitted photoelectron for two different electric-field strengths $E_0 = 10$ a.u. [Fig. 2(a)] and $E_0 = 400$ a.u. [Fig. 2(b)], corresponding to a weak ($U_p = 0.01$ a.u.) and a strong ($U_p = 16$ a.u.) laser field, respectively. Two (multiphoton) peaks which correspond to the net absorption of one and two photons from the field are depicted, as well as a low-energy structure [12] near the ionization threshold. Again, no pronounced differences in the distributions obtained with Hamiltonians (6) and (7) are exhibited. Furthermore, the effect of the diamagnetic term in Eq. (5) is most expressed in the low-energy part of the spectra, giving rise to a higher ionization yield, in agreement with the findings in Fig. 1(a). As it turns out, the relatively large nondipole yield at low kinetic energy electrons can be attributed to the $\boldsymbol{A}^2$ interaction solely, i.e., it would still be present if the $\boldsymbol{A} \cdot \boldsymbol{p}$ term were disregarded completely. Remarkably, even at the lowest field strength considered, corresponding to an electron ponderomotive energy of only 0.01 a.u., the low-energy yield is still significant. The explanation for this surprising behavior is twofold: First, we recognize that the nondipole component of the field associated with the diamagnetic interaction mimics a

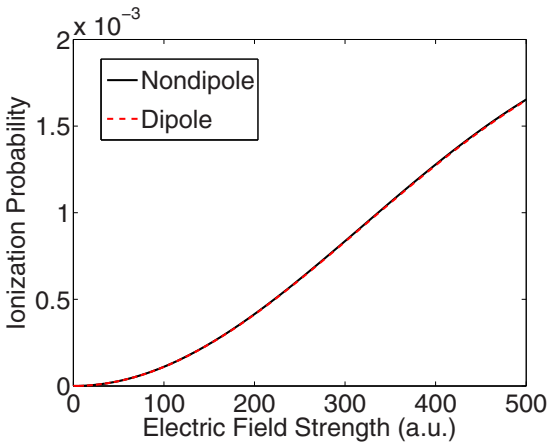

FIG. 3. Total probability for the net absorption of one photon from the laser field (i.e., differential probability integrated over the electron energies $25 < E < 75$ a.u.) vs electric-field strength for a 15-cycle laser pulse with $\omega = 50$ a.u. The solid black line shows the (full) nondipole result obtained by solving the TDSE with the Hamiltonian in Eq. (5) and the dashed red line the dipole approximation result obtained by solving the TDSE with the Hamiltonian in Eq. (7).

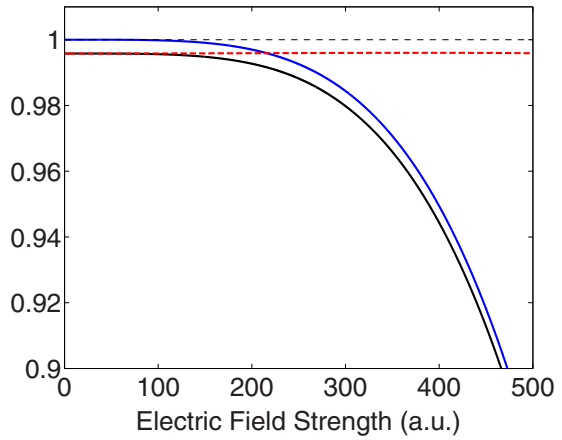

FIG. 4. Projections corresponding to the net absorption of one photon from the laser field as a function of the electric-field strength (see the main text for details). The solid black line shows Eq. (19), the solid blue line Eq. (20), and the dashed red line Eq. (21).

so-called half-cycle nonzero displacement pulse [17] and second, for such pulses the corresponding ionization yield is effectively increased with respect to an ordinary zero-displacement pulse [9]. The reason for the increase is that the electron is pushed away from the nucleus due to the radiation pressure.

Although the multiphoton peaks in Fig. 2 are seemingly less affected by the nondipole field, for the highest intensity the one- and two-photon peaks are somewhat perturbed. Then the following natural question arises: Does the beyond-dipole ionization dynamics alter the multiphoton ionization yields, i.e., integrated probability of absorption of one and/or two photons from the field? Figure 3 gives an answer to this question. The figure shows the total probability for the net absorption of one photon, i.e., the differential probability integrated over the electron energies $25 < E < 75$ a.u. as a function of the electric-field strength. As the dipole and nondipole results essentially coincide in the figure, we may conclude that the beyond-dipole dynamics does not alter the multiphoton ionization yields to any high degree. Now, based on the findings in Figs. 2 and 3 and the close agreement between the obtained results, it seems a likely possibility that multiphoton ionization processes are less prone to nondipole effects. However, as we will see below, this is not necessarily the case.

In order to investigate the multiphoton ionization peaks in more detail and the role of nondipole effects in particular, we now aim at measuring differences in the respective final wave functions, as obtained with the Hamiltonians (5)–(7). This is achieved in the following way. First, the wave function corresponding to the absorption of one photon from the field is extracted from the total wave packet, i.e., we collect the part of the wave function representing electron continuum energies in the interval $25 < E < 75$ a.u. Second, the extracted wave functions are normalized to one and they are denoted by $|\Psi_{\text{Eq. (5)}}\rangle$, $|\Psi_{\text{Eq. (6)}}\rangle$, and $|\Psi_{\text{Eq. (7)}}\rangle$, corresponding to solving the TDSE with the Hamiltonians (5), (6), and (7), respectively. Finally, the projections

$$|\langle\Psi_{\text{Eq. (7)}}|\Psi_{\text{Eq. (5)}}\rangle|^2, \tag{19}$$

$$|\langle\Psi_{\text{Eq. (6)}}|\Psi_{\text{Eq. (5)}}\rangle|^2, \tag{20}$$

and

$$|\langle\Psi_{\text{Eq. (7)}}|\Psi_{\text{Eq. (6)}}\rangle|^2 \tag{21}$$

are made and the results are presented in Fig. 4.

From the result obtained with Eq. (19), it is evident that the one-photon resonance is strongly affected by beyond-dipole dynamics and in particular for field strengths beyond $E_0 \simeq 100$ a.u. Furthermore, comparing the projections (19) and (20) in Fig. 4, it is clear that it is the diamagnetic interaction, as represented by the $\boldsymbol{A}^2$ operator in Eqs. (3) and (5), that is responsible for the most important correction for the higher field strengths. Nonetheless, for the lower field strengths, i.e., for $E_0 \lesssim 100$ a.u., the $\boldsymbol{A}^2$ term becomes unimportant as far as the one-photon resonance is concerned and it is the spatial dependence in the $\boldsymbol{A} \cdot \boldsymbol{p}$ term in Eqs. (3) and (6) that takes over as the dominating nondipole channel. [Note, however, that the $\boldsymbol{A}^2$ interaction is still important when it comes to the bound-state excitation dynamics, as was already demonstrated in Fig. 1(c).] Very interestingly, the last projection (21), as indicated with the dashed red line in Fig. 4, clearly shows that the nondipole effect due to the $\boldsymbol{A} \cdot \boldsymbol{p}$ operator is largely independent of the laser intensity, as the correction remains constant all the way from the perturbative limit to the strongest fields considered. Although these beyond-dipole corrections turn out to be small in the present case, the results clearly demonstrate the fact that the dipole approximation, i.e., the long-wavelength approximation, breaks down at very high photon energies, even in the perturbative limit.

The next question is whether the predicted nondipole effects, as visualized in Fig. 4, can be measured in some way. The answer is positive and is demonstrated in Figs. 5 and 6. The figures depict the angular distribution of the emitted photoelectron for various scenarios. First, Fig. 5 shows the

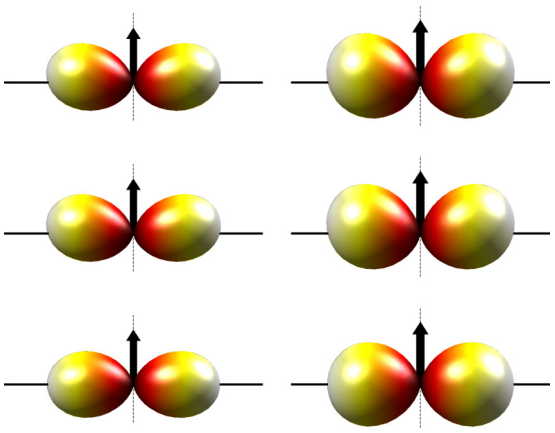

FIG. 5. Electron angular distributions, integrated over the electron energy interval $25 < E < 75$ a.u. (corresponding to the net absorption of one photon from the field), for $\omega = 50$ a.u., a 15-cycle laser pulse linearly polarized in the horizontal direction and propagating in the upward direction (indicated with an arrow), and two different electric-field strengths: $E_0 = 10$ a.u. (left column) and $E_0 = 400$ a.u. (right column). The top panels show the (full) nondipole result obtained by solving the TDSE with the Hamiltonian in Eq. (5), the middle panels the nondipole result obtained by solving the TDSE with only the $\boldsymbol{A} \cdot \boldsymbol{p}$ term, i.e., the Hamiltonian in Eq. (6), and the bottom panels the corresponding dipole result obtained by solving the TDSE with the Hamiltonian in Eq. (7).

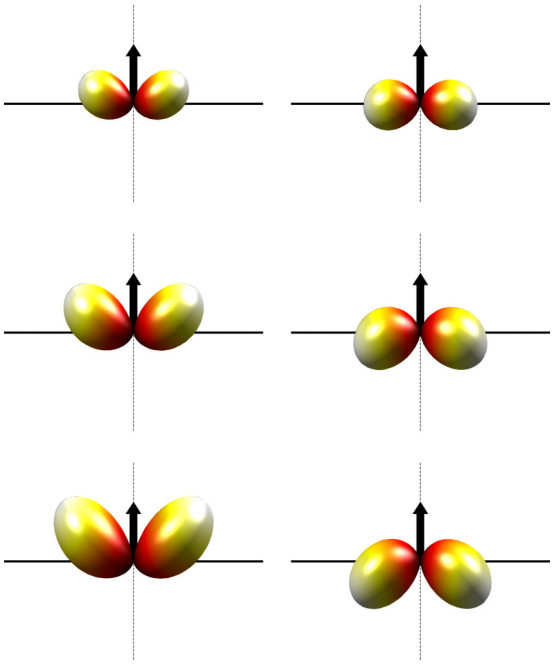

FIG. 6. Full (nondipole) electron angular distributions for a 15-cycle laser pulse linearly polarized in the horizontal direction and propagating in the upward direction (indicated with an arrow) and for three different electric-field strengths: $E_0 = 400$ a.u. (top panels), $E_0 = 500$ a.u. (middle panels), and $E_0 = 600$ a.u. (bottom panels). The left column shows the angular distribution as obtained by integrating over the energies corresponding to the low-energy side of the one-photon resonance, i.e., $25 < E < 49.1$ a.u., and the right column the angular distribution as obtained by integrating over the energies corresponding to the high-energy side of the one-photon resonance, i.e., $49.1 < E < 75$ a.u. The total (integrated) one-photon ionization yields are 0.0013, 0.0017 and 0.0019, in the top, middle, and bottom panels, respectively.

distribution corresponding to the net absorption of one photon from the field, (i.e., the differential probability integrated over the electron energies $25 < E < 75$ a.u.) and for two different field strengths $E_0 = 10$ a.u. (left panels) and $E_0 = 400$ a.u. (right panels). The top, middle, and bottom panels represent the results of the Hamiltonians (5), (6), and (7), respectively. For both the weak- and strong-field cases, Eqs. (5) and (6) produce very similar results and the breakdown of the dipole approximation is manifested as a (weak) bending of the angular lobes in the laser propagation direction (upward). Nevertheless, the measured effect is quite small and it turns out to be rather independent of the laser intensity. As such, it is mainly the effect of the $\boldsymbol{A} \cdot \boldsymbol{p}$ nondipole corrections that is expressed in the figure. This finding may seem contradictory to the results in Fig. 4, where it was clearly demonstrated that the diamagnetic term is the most important one with respect to beyond-dipole ionization dynamics.

Finally, Fig. 6 shows that the one-photon resonance is indeed strongly influenced by beyond-dipole ionization dynamics induced by the diamagnetic interaction, in accord with Fig. 4. Figure 6 depicts angular distributions for the three different (strong) field strengths $E_0 = 400$ a.u. (top panels), $E_0 = 500$ a.u. (middle panels), and $E_0 = 600$ a.u. (bottom panels). The left-side panels are the results obtained when integrating over the electron energies $25 < E < 49.1$ a.u., i.e., by summing over the energies corresponding to the low-energy (left-hand) side of the one-photon resonance. Likewise, the right-side panels represent the corresponding angular distributions calculated from the high-energy (right-hand) side of the resonance, as integrated over the electron energies $49.1 < E < 75$ a.u. Very interestingly, the left-hand side distributions are bent in the forward (laser propagation) direction, whereas the right-hand side ones are bent in the backward (counterpropagation) direction. The bending increases with increasing laser intensity. Although not explicitly shown here, we have also checked that the higher multiphoton ionization peaks express a very similar behavior. Furthermore, we have found that this left-right asymmetry of the resonances is a general phenomenon, i.e., the same pattern is repeated for both lower and higher photon energies in the x-ray regime as well as for shorter and longer pulse durations.

The bending of the angular lobes in the laser propagation and/or counterpropagation directions can be explained within the framework of a simple model which bears a clear resemblance to the so-called strong-field approximation (SFA) model, also known as the Keldysh-Faisal-Reiss theory [31–33]. At the heart of this model is an assumption that the Coulomb interaction can be neglected once the electron is in the continuum. Likewise, the perturbation due to the laser field is neglected in the initial (bound) state. Neglecting the Coulomb potential, the Hamiltonian describing a free electron moving in the (nondipole) laser field is given by

$$H = \frac{p^2}{2m} + \frac{e}{m}\boldsymbol{A}(t) \cdot \boldsymbol{p} - \frac{e^2}{mc}\boldsymbol{A}(t) \cdot \frac{\partial \boldsymbol{A}(t)}{\partial t}\hat{\boldsymbol{k}} \cdot \boldsymbol{r}. \qquad (22)$$

Note that here only the leading-order correction beyond the dipole approximation is retained, i.e., the $\boldsymbol{A}^2$ term is expanded to first order in $\boldsymbol{\kappa}\cdot\boldsymbol{r}$, and any unimportant and purely time-dependent factors have been omitted [cf. Eq. (8)]. The Hamiltonian (22) is the same as (9), except that the spatial dependence in the $\boldsymbol{A}\cdot\boldsymbol{p}$ operator and the Coulomb potential have been omitted. The analytical solutions to the TDSE (1) with the Hamiltonian (22) are the so-called Volkov wave functions describing a free electron with momentum $\boldsymbol{p}=\hbar\boldsymbol{k}$ moving in the electromagnetic field,

$$\Psi_{\boldsymbol{k}}^{V}(\boldsymbol{r},t)=\frac{1}{(2\pi)^{3/2}}\exp\left(i\left[\boldsymbol{k}+\frac{e^2}{2mc\hbar}A^2(t)\hat{\boldsymbol{\kappa}}\right]\cdot\boldsymbol{r}\right.$$
$$\left.-i\boldsymbol{k}\cdot\boldsymbol{\alpha}(t)-i\beta(t)\right), \tag{23}$$

where

$$\beta(t)=\frac{\hbar}{2m}\int_{t_0}^{t}\left[\boldsymbol{k}+\frac{e^2}{2mc\hbar}A^2(t')\hat{\boldsymbol{\kappa}}\right]^2 dt' \tag{24}$$

and

$$\boldsymbol{\alpha}(t)=\frac{e}{m}\int_{t_0}^{t}\boldsymbol{A}(t')dt' \tag{25}$$

is the time-dependent displacement vector of a corresponding (classical) free electron oscillating in the (dipole) laser field. The normalization condition is chosen so that the Volkov states are normalized to a δ function. Then, according to first-order time-dependent perturbation theory, the time-dependent transition amplitude $c(\boldsymbol{k},t)$ from the initial $\Psi_{1s}(\boldsymbol{r},t)=\psi_{1s}(\boldsymbol{r})e^{-iE_{1s}t/\hbar}$ ground state to some final continuum state of momentum $\boldsymbol{p}=\hbar\boldsymbol{k}$ is simply given by

$$c(\boldsymbol{k},t)=\frac{e}{i\hbar m}\int_{-\infty}^{t}\langle\Psi_{\boldsymbol{k}}^{V}(t')|\boldsymbol{A}(t')\cdot\boldsymbol{p}|\Psi_{1s}(t')\rangle dt'. \tag{26}$$

Aiming at keeping the model as simple as possible while still being capable of describing the main mechanism behind the bending of the angular lobes in Fig. 6, note at this point that only the electric dipole interaction has been taken into account in the coupling between the initial bound state and the continuum states in Eq. (26). As such, perturbations due to the beyond-dipole interactions are only included in the final continuum states [cf. Eq. (23)]. Finally, the momentum-resolved ionization probability at the end of the laser pulse, i.e., at time $t=T$, is computed as

$$\frac{dP}{d\boldsymbol{k}}=|c(\boldsymbol{k},T)|^2. \tag{27}$$

Figure 7 depicts (integrated) electron angular distributions similar to the ones shown in Fig. 6, but now instead calculated based on the model (27), with $E=\frac{1}{2}k^2$. Except for a somewhat higher total yield, there is a clear resemblance between the results in Figs. 6 and 7. This means that the comparably simple model framework actually captures the main mechanism behind the ejection dynamics. Now inspecting Eqs. (23) and (24) it is clear that the beyond-dipole correction term, which is proportional to $A^2(t)$, gives rise to an instantaneous (positive) momentum shift of the continuum states in the laser propagation (forward) direction. In effect, Volkov states

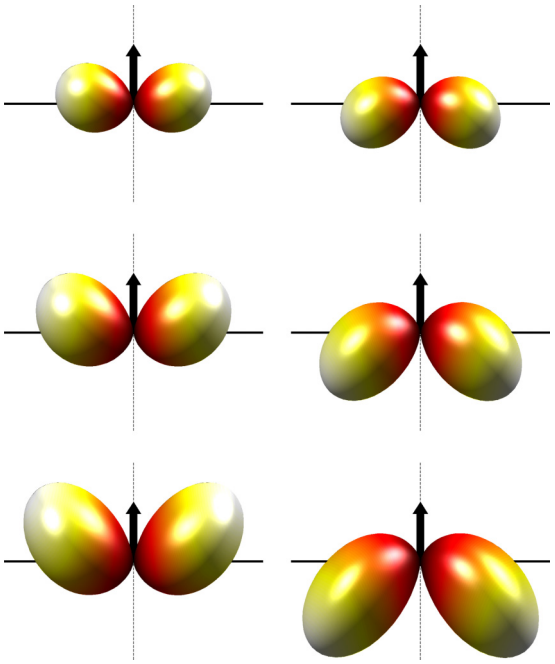

FIG. 7. Same as Fig. 6, but for the corresponding results obtained with the simple model (26). The total (integrated) one-photon ionization yields are 0.0018, 0.0025 and 0.0030, in the top, middle, and bottom panels, respectively.

with $\boldsymbol{k}\cdot\hat{\boldsymbol{\kappa}}<0$ are downshifted in energy due to this ac Stark shift, while states with $\boldsymbol{k}\cdot\hat{\boldsymbol{\kappa}}>0$ are upshifted. As such, the (instantaneous) resonance condition for the absorption of one photon from the field will be met at different energies depending on whether the electron is emitted in the forward or backward direction, respectively. Ultimately, this explains why the electron tends to be emitted in the laser propagation direction for energies corresponding to the low-energy side of the (multi)photon resonance, while it is more likely to be emitted in the opposite direction for energies corresponding to the high-energy side of the resonance.

Finally, inspecting the one-photon resonance in some more detail, in Fig. 8 we present the extracted double differential angular and energy probability $\partial^2P/\partial\Omega\partial E$ for emitting a photoelectron with energy E into the solid angle Ω, as obtained for a set of discrete electron energies evenly distributed about the photoelectron peak, i.e., for energies in the range from 45 to 53 a.u. in steps of 1 a.u. of energy. The left column depicts the results of the full calculations, whereas the right column shows the corresponding results calculated based on the simple (SFA) model (27). In both cases the electric-field strength $E_0=400$ a.u. The figure clearly displays the evolution of the degree of bending of the angular lobes in the laser propagation and/or counterpropagation directions with respect to the kinetic energy of the emitted photoelectron. Note again the clear resemblance of the full and approximate results, at least at the qualitative level. As a matter of fact, the small discrepancies observed in the respective results can to a large extent be explained by the fact that the spatial dependence in the vector potential in the $\boldsymbol{A}\cdot\boldsymbol{p}$ operator was not taken into account in the SFA model.

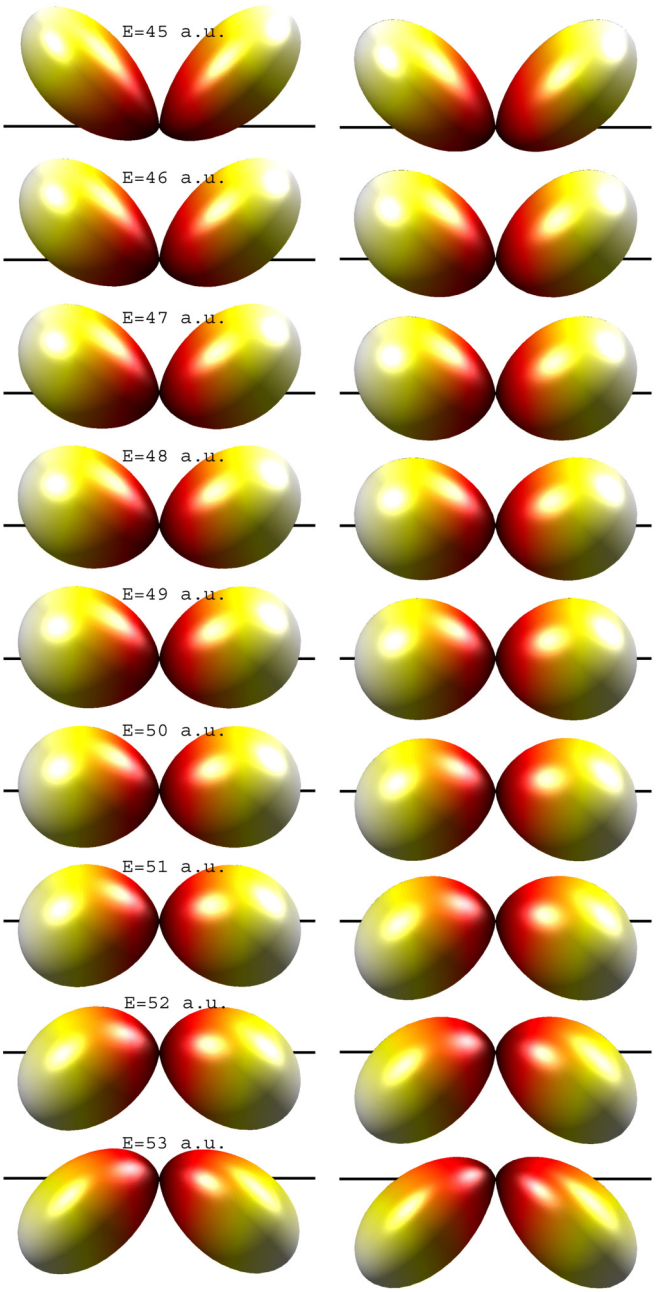

FIG. 8. Double differential angular and energy probability $\partial^2 P/\partial\Omega\partial E$ extracted at the final continuum electron energies as indicated in the figure, i.e., for energies ranging from 45 to 53 a.u. (from top to bottom) in steps of 1 a.u. The laser pulse is the same as before with $E_0 = 400$ a.u. The left column shows the *ab initio* result and the right column the simple model (SFA) result calculated by means of Eq. (26).

IV. CONCLUSION

We have studied the role of the spatial dependence of a 1.36-keV x-ray laser pulse in the ionization and excitation of ground-state hydrogenic atoms. The resulting beyond-dipole (nondipole) dynamics of the system in response to the laser field was analyzed in some detail, and similarities to and differences from the widely used dipole approximation were pointed out. Furthermore, the relative importance of the diamagnetic interaction ($\boldsymbol{A}^2$) in comparison with the $\boldsymbol{A}\cdot\boldsymbol{p}$ light-matter interaction was pinpointed. Although only one particular scenario was considered in the present work, i.e., a 15-cycle laser field of angular frequency $\omega = 50$ a.u., the main findings are expected to be of some general validity, and we have explicitly checked that very similar conclusions can be drawn at both somewhat lower and higher laser frequencies in the x-ray regime.

An important observation of the study is that the beyond-dipole correction as induced by the spatial dependence in the $\boldsymbol{A}\cdot\boldsymbol{p}$ operator was found to be largely *independent* of the laser intensity, all the way from the perturbative limit to the weakly relativistic regime. Furthermore, it was found that the $\boldsymbol{A}^2$ operator is by far the most important one when it comes to nondipole excitation and ionization dynamics in strong fields, in agreement with the conclusions previously drawn in the extreme ultraviolet (as well as vuv) regime [2,3,12]. It was also found that the linear approximation to the Hamiltonian (9), i.e., keeping only the leading-order corrections beyond the dipole approximation, is sufficient to capture essentially all the features of the nondipole light-matter interaction.

Strictly speaking, the dipole approximation was not expected to be very accurate for the comparably high photon energy considered in this work, merely due to the short wavelength of the laser light. In spite of this, the beyond-dipole corrections were found to be small in the perturbative limit and any differences were manifested in the angular resolved probability distributions as a characteristic bending of the angular (dipole) lobes in the laser propagation direction (cf. Fig. 5). For stronger fields the situation changes dramatically: The diamagnetic interaction suddenly switches on, the magnetic-field component of the laser field becomes important, and the ionization-excitation dynamics is strongly perturbed. The resulting increase in the ionization yields primarily leads to the emission of low-energy electrons, whereas the corresponding multiphoton ionization peaks are seemingly much less sensitive to nondipole effects.

Taking an even closer look at the multiphoton resonances reveals a different story, in that a characteristic and strong forward-backward asymmetry in the respective electron angular distributions is exhibited in the intense field limit. Focusing on the one-photon resonance first, for electron energies $E < \hbar\omega - I_p$ (I_p is the ionization potential), corresponding to the low-energy side of the resonance peak, the electron is found to be most likely emitted in the laser propagation (forward) direction, whereas for $E > \hbar\omega - I_p$, i.e., the high-energy side of the resonance, the situation turns and the electron tends to be emitted in the counterpropagation (backward) direction. As it turns out, similar conclusions also hold for the higher-order multiphoton ionization resonances. Finally, it was found that the general mechanism behind the observed forward-backward asymmetries in the angular distributions could be explained in terms of a comparably simple semianalytical model, emphasizing the importance of the ac Stark shift of the final continuum states, due to both the dipole and nondipole fields, as the source of the observed features.

[1] A. Bugacov, M. Pont, and R. Shakeshaft, Phys. Rev. A **48**, R4027 (1993).

[2] N. J. Kylstra, R. A. Worthington, A. Patel, P. L. Knight, J. R. Vázquez de Aldana, and L. Roso, Phys. Rev. Lett. **85**, 1835 (2000).

[3] J. R. Vázquez de Aldana, N. J. Kylstra, L. Roso, P. L. Knight, A. Patel, and R. A. Worthington, Phys. Rev. A **64**, 013411 (2001).

[4] M. Førre, S. Selstø, J. P. Hansen, and L. B. Madsen, Phys. Rev. Lett. **95**, 043601 (2005).

[5] M. Førre, J. P. Hansen, L. Kocbach, S. Selstø, and L. B. Madsen, Phys. Rev. Lett. **97**, 043601 (2006).

[6] M. Førre, S. Selstø, J. P. Hansen, T. K. Kjeldsen, and L. B. Madsen, Phys. Rev. A **76**, 033415 (2007).

[7] M. Førre, Phys. Rev. A **74**, 065401 (2006).

[8] K. J. Meharg, J. S. Parker, and K. T. Taylor, J. Phys. B **38**, 237 (2005).

[9] D. Dimitrovski, M. Førre, and L. B. Madsen, Phys. Rev. A **80**, 053412 (2009).

[10] M. Y. Emelin and M. Y. Ryabikin, Phys. Rev. A **89**, 013418 (2014).

[11] M. Y. Ryabikin and A. M. Sergeev, Opt. Express **7**, 417 (2000).

[12] M. Førre and A. S. Simonsen, Phys. Rev. A **90**, 053411 (2014).

[13] A. S. Simonsen and M. Førre, Phys. Rev. A **92**, 013405 (2015).

[14] H. Bachau, M. Dondera, and V. Florescu, Phys. Rev. Lett. **112**, 073001 (2014).

[15] M. Førre and A. S. Simonsen, Phys. Rev. A **93**, 013423 (2016).

[16] A. S. Simonsen and M. Førre, Phys. Rev. A **93**, 063425 (2016).

[17] A. S. Simonsen, T. Kjellsson, M. Førre, E. Lindroth, and S. Selstø, Phys. Rev. A **93**, 053411 (2016).

[18] S. Chelkowski, A. D. Bandrauk, and P. B. Corkum, Phys. Rev. A **92**, 051401(R) (2015).

[19] S. Selstø, E. Lindroth, and J. Bengtsson, Phys. Rev. A **79**, 043418 (2009).

[20] A. Di Piazza, C. Müller, K. Z. Hatsagortsyan, and C. H. Keitel, Rev. Mod. Phys. **84**, 1177 (2012).

[21] Y. I. Salamin, S. X. Hu, K. Z. Hatsagortsyan, and C. H. Keitel, Phys. Rep. **427**, 41 (2006).

[22] T. Kjellsson, M. Førre, A. S. Simonsen, S. Selstø, and E. Lindroth, Phys. Rev. A **96**, 023426 (2017).

[23] T. Kjellsson, S. Selstø, and E. Lindroth, Phys. Rev. A **95**, 043403 (2017).

[24] H. Bauke, H. G. Hetzheim, G. R. Mocken, M. Ruf, and C. H. Keitel, Phys. Rev. A **83**, 063414 (2011).

[25] C. T. L. Smeenk, L. Arissian, B. Zhou, A. Mysyrowicz, D. M. Villeneuve, A. Staudte, and P. B. Corkum, Phys. Rev. Lett. **106**, 193002 (2011).

[26] A. Ludwig, J. Maurer, B. W. Mayer, C. R. Phillips, L. Gallmann, and U. Keller, Phys. Rev. Lett. **113**, 243001 (2014).

[27] M. Dondera, V. Florescu, and H. Bachau, Phys. Rev. A **90**, 033423 (2014).

[28] M. Dondera and H. Bachau, Phys. Rev. A **85**, 013423 (2012).

[29] H. R. Varma, M. F. Ciappina, N. Rohringer, and R. Santra, Phys. Rev. A **80**, 053424 (2009).

[30] M. K. Gordon and L. F. Shampine, in *Proceedings of the 1974 Annual Conference, ACM '74* (ACM, New York, 1974), Vol. 1, pp. 46–53.

[31] L. V. Keldysh, Zh. Eksp. Teor. Fiz. **47**, 1945 (1964) [Sov. Phys. JETP **20**, 1307 (1965)].

[32] F. H. M. Faisal, J. Phys. B **6**, L89 (1973).

[33] H. R. Reiss, Phys. Rev. A **22**, 1786 (1980).